

Spiral spin structure in the Heisenberg pyrochlore magnet CdCr_2O_4

M. Matsuda, M. Takeda, M. Nakamura, and K. Kakurai

Quantum Beam Science Directorate, Japan Atomic Energy Agency (JAEA), Tokai, Ibaraki 319-1195, Japan

A. Oosawa

Department of Physics, Sophia University, 7-1 Kioi-cho, Chiyoda-ku, Tokyo 102-8554, Japan

E. Lelièvre-Berna

Institut Laue Langevin, BP 156, F-38402 Grenoble Cedex 9, France

J.-H. Chung

*Department of Materials Science and Engineering, University of Maryland, College Park, Maryland 20742, USA
and NIST Center for Neutron Research, National Institute of Standards and Technology, Gaithersburg, Maryland 20899-8562, USA*

H. Ueda

The Institute for Solid State Physics, The University of Tokyo, Kashiwa, Chiba 277-8581, Japan

H. Takagi

*Graduate School of Frontier Science, The University of Tokyo, Kashiwa, Chiba 277-8562, Japan
and RIKEN (The Institute of Physical and Chemical Research), Wako, Saitama 351-0198, Japan*

S.-H. Lee

*Department of Physics, University of Virginia, 382 McCormick Road, Charlottesville, Virginia 22904-4714, USA
(Received 9 November 2006; published 20 March 2007)*

A frustrated spinel CdCr_2O_4 undergoes a three-dimensional spin-Peierls transition at $T_N=7.8$ K from a cubic paramagnetic to a tetragonal Néel state. The Néel state has a spiral magnetic structure with a characteristic wave vector of $(0, \delta, 1)$ when the c axis is elongated [J.-H. Chung *et al.*, Phys. Rev. Lett. **95**, 247204 (2005)]. Here, we report our spherical neutron polarimetry experiments to investigate the spiral spin structure in detail. Our results indicate that the spins lie in the ac plane perpendicular to the direction of the spiral modulation. We also find that the spiral structure in the ac plane is elliptical with the c component larger by $\sim 24\%$ than the a component, suggesting a strong coupling between the magnetic structure and the structural distortion. Unpolarized neutron diffraction under an external magnetic field has also been performed. The magnetic-field dependence suggests the existence of magnetic anisotropy in the Néel state, which is consistent with our previous inelastic studies [J.-H. Chung *et al.*, Phys. Rev. Lett. **95**, 247204 (2005)].

DOI: 10.1103/PhysRevB.75.104415

PACS number(s): 75.10.Jm, 75.25.+z, 75.50.Ee

I. INTRODUCTION

Cr-based spinels ACr_2O_4 ($A=\text{Mg, Zn, Cd, and Hg}$) have attracted much attention because the magnetic Cr^{3+} ($S=\frac{3}{2}$) ions form the most frustrated lattice, a network of corner-sharing tetrahedra.¹⁻⁵ Furthermore, due to the direct overlap of t_{2g} orbitals of neighboring Cr^{3+} ions ($3d^3$), the spin Hamiltonian has the dominant isotropic antiferromagnetic nearest-neighbor interactions. The resulting strong frustration suppresses the system from ordering down to a much lower temperature than the Curie-Weiss temperature, Θ_{CW} .^{6,7} Consequently, ACr_2O_4 remains paramagnetic to temperatures far below $|\Theta_{CW}|=390$ K and 88 K for $A=\text{Zn}$ (Ref. 8) and Cd,^{5,9,10} respectively. Upon further cooling, however, they undergo a first-order three-dimensional spin-Peierls phase transition from a cubic paramagnetic state to a tetragonal Néel state.

One of the central issues in the field of geometrical frustration is the understanding of which spin structure to be selected as the ground state out of the macroscopically degenerate ground-state manifolds, under what circumstances,

and by what mechanism. Not much progress has been made for ACr_2O_4 in this regard mainly because the ground states often have complex spin structures. For instance, the Néel state of ZnCr_2O_4 ($T_N=T_{st}=12.0$ K, where T_N and T_{st} are the Néel temperature and structural transition temperature, respectively, with $a > c$ below T_{st}) has multiple characteristic wave vectors $\mathbf{Q}=(\frac{1}{2}, \frac{1}{2}, 0)$, $(1, 0, \frac{1}{2})$, $(\frac{1}{2}, \frac{1}{2}, \frac{1}{2})$, and $(0, 0, 1)$. Furthermore, the relative neutron-scattering intensities of these wave vectors are sample dependent.¹¹ This indicates that the system is very close to a critical point around many different spin structures in the phase space. The commensurate wave vectors and weak tetragonal distortion make it difficult to distinguish different crystals as well as spin domains.

Recently, we have reported our neutron-scattering study of CdCr_2O_4 that is also in the long range order at temperatures below $T_N=T_{st}=7.8$ K.¹² Our study showed that unlike in ZnCr_2O_4 , in CdCr_2O_4 the lattice elongates along the c axis and the magnetic structure has an incommensurate (IC) order. The high \mathbf{Q} resolution data indicated that the IC magnetic structure has a single characteristic wave vector of

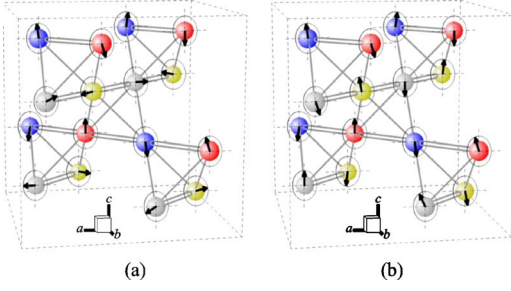


FIG. 1. (Color online) Two possible spin structures of CdCr_2O_4 : (a) nearly orthogonal stacking and (b) nearly collinear stacking along the c axis. The spin spirals have ellipticity elongated along the c axis as discussed in the text. The magnetic lattice with the characteristic wave vector of \mathbf{Q}_M consists of four independent sublattices, as represented by spheres with different colors.

$\mathbf{Q}_M=(0, \delta, 1)$ with the incommensurability $\delta \sim 0.09$ perpendicular to the unique c axis. Combining the elastic and inelastic measurements, overall magnetic structures were proposed, as shown in Fig. 1. Spins form spirals with equal pitches along chains on the ab plane, while the stacking along the c axis may be either nearly orthogonal [Fig. 1(a)] or nearly collinear [Fig. 1(b)].

In this paper, we report detailed studies on the spin structure of CdCr_2O_4 using the spherical neutron polarimetry technique. The following are our main findings: (1) the ac plane that is perpendicular to the incommensurability direction is an easy plane, (2) the spiral structure is elliptic with the c component larger, and (3) the magnetic chirality domains with clockwise and counterclockwise spirals have unequal populations. We have also performed unpolarized neutron-diffraction measurements under a magnetic field (H). The H dependence can be qualitatively explained by domain reorientations. The data also reveal critical fields depending on the H directions, which may correspond to the anisotropy along these directions.

II. EXPERIMENTAL DETAILS

A single crystal that has a shape of a thin plate and weighs ~ 100 mg was grown by flux method. Since natural Cd has a large neutron-absorption cross section, a single crystal enriched with ^{114}Cd was used. The neutron elastic scattering experiments were carried out on the thermal neutron three-axis spectrometers TAS-1 and TAS-2 installed at JRR-3 at Japan Atomic Energy Agency and on the cold neutron three-axis spectrometers SPINS installed at NIST. Contamination from higher-order beams is effectively eliminated using a PG filter at TAS-1 and TAS-2 and a Be filter at SPINS. Polarized neutron-diffraction measurements were performed using CRYOPAD installed on TAS-1.¹³ Heusler alloy (111) crystals were used as monochromator and analyzer. A flipping ratio of ~ 30 was measured at the nuclear (400) reflection, corresponding to 94% polarization of the beam. The incident neutron energy was fixed at $E_i=14.7$ meV. The horizontal collimator sequence was open-80'-S-80'-open. The neutron elastic scattering experiments under a magnetic field, using split-pair superconducting magnets, were performed on

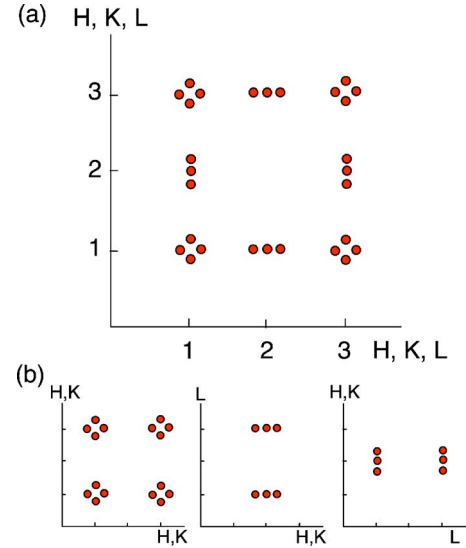


FIG. 2. (Color online) (a) The observed pattern of the magnetic Bragg reflections on the scattering plane. (b) The observed reflections are decomposed into three groups depending on the direction of the c axis. The central peaks of the triplets are tails of the doublets that are present above and below the scattering plane. Therefore, the quartets are always in the ab plane.

TAS-2 and SPINS, using fixed incident neutron energies of 14.7 meV (TAS-2) and 5.0 meV (SPINS). The horizontal collimator sequence was guide-80'-S-80'-open on TAS-2. A two-dimensional (2D) position-sensitive detector (PSD) was placed just after the second collimator on SPINS. The collimator sequence was guide-80' (horizontal)-S-40' (vertical).

III. RESULTS

A. Domain structure in CdCr_2O_4

In the tetragonal phase, there are three crystallographic domains so that $(hk0)$, $(h0l)$, and $(0kl)$ zones can be observed in the same scattering plane. Figure 2 indicates schematically the IC magnetic peak positions.¹² Since there exist three crystallographic and two magnetic k domains, in which IC vectors are different, there are six magnetic domains in total. The magnetic Bragg peaks with $\mathbf{Q}_M=(0, \delta, 1)$, $(\delta, 0, 1)$, $(1, 0, \delta)$, $(1, \delta, 0)$, $(0, 1, \delta)$, and $(\delta, 1, 0)$, with $\delta \sim 0.09$, from the six magnetic domains are observed in one scattering plane, as shown in Fig. 2(a). The observed reflections are decomposed into three groups depending on the direction of the c axis as shown in Fig. 2(b). There are two kinds of IC peak structures; triplet and quadruplet. The quadruplet originates from the scattering in the $(hk0)$ plane. Since h and k are equivalent in the tetragonal phase, the modulation vector can go along both the a and b axes. On the other hand, the triplet originates from the scattering in the $(h0l)$ and $(0kl)$ plane's with the c axis in the scattering plane and also perpendicular to the direction along which the three peaks form a line. The central peak does not come from the scattering at the commensurate position in the scattering plane, but it comes from the IC peaks that reside above and below the scattering plane. The scattering intensity is not so small because of the

poor instrumental vertical \mathbf{Q} resolution. From now on, the central peak will be called the vertical IC peak, and the other peaks the horizontal IC peaks, according to the orientation of the reflections to the scattering plane.

The magnetic lattice with the characteristic wave vector of \mathbf{Q}_M consists of four independent sublattices, as shown by spheres with different colors in Fig. 1. Each sublattice connects all third nearest-neighboring Cr^{3+} ions that are separated by the symmetrically equivalent distances of $(\frac{1}{2}, \frac{1}{2}, 0)$. They are the second nearest-neighbors along the chains represented by the lines in Fig. 1. There are two possible spin arrangements along the c axis. One is the almost orthogonal stacking, as shown in Fig. 1(a). Another is the almost collinear stacking along the c axis, as shown in Fig. 1(b). It is suggested that the former structure better explains the observed spin wave excitations.

B. Spherical neutron polarimetry experiments

The spherical neutron polarimetry technique is the most powerful tool in determining a magnetic structure because it measures polarization in any arbitrary direction.^{14–18} For our measurements, the incident polarization was chosen to be in three orthogonal directions x , y , and z , where x is defined to be along the scattering vector, y is defined to be in the scattering plane perpendicular to x direction, and z is defined to be perpendicular to the scattering plane. The polarization of the scattered beam was also analyzed in the three directions, thus giving nine polarization tensor terms for each peak P_{if} , with $i, f = x, y$, and z , where i and f represent “initial” and “final,” respectively. P_{if} is defined as

$$P_{if} = \frac{I_{+i,+f} - I_{+i,-f}}{I_{+i,+f} + I_{+i,-f}},$$

where $I_{i,f}$ represents the scattering intensity with initial and final polarizations i and f , respectively. The polarization of the scattered beam can be expressed as follows:

$$\mathbf{P}_f = \frac{2[(\mathbf{P}_i \mathbf{A}) \mathbf{A} + (\mathbf{P}_i \mathbf{B}) \mathbf{B}] - (\mathbf{A}^2 + \mathbf{B}^2) \mathbf{P}_i + 2(\mathbf{A} \times \mathbf{B})}{\mathbf{A}^2 + \mathbf{B}^2 - 2\mathbf{P}_i \cdot (\mathbf{A} \times \mathbf{B})}, \quad (1)$$

where $\mathbf{M}(\mathbf{Q})$ is the magnetic structure factor

$$\mathbf{M}(\mathbf{Q}) = \sum_j \langle \mathbf{S}_{j\perp} \rangle e^{i\mathbf{Q} \cdot \mathbf{r}_j} = \mathbf{A} + i\mathbf{B},$$

and \mathbf{P}_i and \mathbf{P}_f are polarization states of incident and scattered beams, respectively. In the spiral structure with a periodicity ~ 11 times the chemical unit cell along the b axis ($\delta = 0.09$), \mathbf{A} and \mathbf{B} can be written as

$$\mathbf{A} = \sum_{j=1}^{11} \langle \mathbf{S}_{j\perp} \rangle \cos\left(\frac{2\pi jk}{11}\right),$$

$$\mathbf{B} = \sum_{j=1}^{11} \langle \mathbf{S}_{j\perp} \rangle \sin\left(\frac{2\pi jk}{11}\right),$$

where $\langle \mathbf{S}_{j\perp} \rangle$ is the spin component perpendicular to \mathbf{Q} .

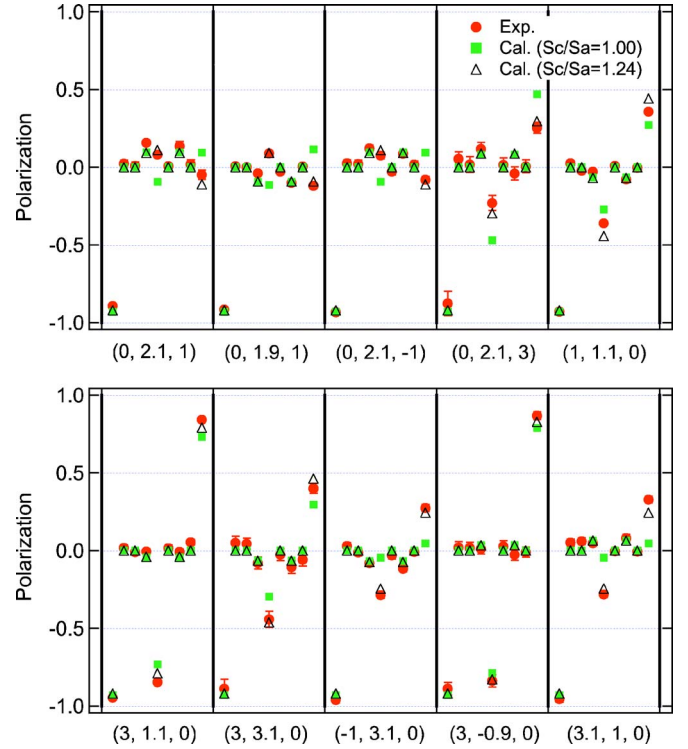


FIG. 3. (Color online) Summary of polarization matrix elements P_{if} at ten magnetic Bragg peaks in CdCr_2O_4 . The symbols represent P_{xx} , P_{xy} , P_{xz} , P_{yx} , P_{yy} , P_{yz} , P_{zx} , P_{zy} , and P_{zz} from left to right. The squares and triangles show the elements calculated for the circular spiral ($S_c/S_a=1$) and the elliptical spiral structure ($S_c/S_a=1.24$), respectively.

These measurements of the polarization were performed at several magnetic peaks, and the results are summarized in Fig. 3. Even without a detailed analysis of these results, a few characteristic features are to be noted in the data: (1) P_{xx} is always almost close to the negative instrumental beam polarization, i.e., ~ -0.92 , indicating the magnetic nature of the observed peaks. (2) The y or z polarized incident beam is almost depolarized, i.e., $P_{yy} \sim P_{zz} \sim 0$, when the scattering vector \mathbf{Q} is almost parallel to the incommensurability vector [e.g., at $\mathbf{Q}=(0, 2.09, 1)$ or $(0, 1.91, 1)$ and at $\mathbf{Q}=(3, 1.09, 0)$ or $(3, -0.91, 0)$]. When \mathbf{Q} is almost perpendicular to the incommensurability vector, y polarized incident neutrons are almost flipped, i.e., $P_{yy} \sim -0.9$, and z polarized incident neutrons are almost not flipped, i.e., $P_{zz} \sim +0.9$. These features directly indicate that the spin structure has a spiral modulation, with the spins lying on the ac plane that is perpendicular to the spiral propagation vector. (3) P_{yx} and P_{zx} are finite, which confirms that the spin structure is spiral, and furthermore, the two chirality domains are unequally populated. It is because the P_{yx} and P_{zx} terms come from the $+2(\mathbf{A} \times \mathbf{B})$ term in Eq. (1) that reflects the chirality of the spiral structure, and they are zero for any collinear spin structure. However, P_{yx} and P_{zx} also become zero if two chirality domains with clockwise and counterclockwise chiralities are distributed equally. These terms can also be negligible if \mathbf{Q} is almost perpendicular to the IC vector as at $\mathbf{Q}=(3, 1.1, 0)$ and $(3, -0.9, 0)$. The finite values of the P_{yx} and P_{zx} terms at

other reflections clearly indicate the spiral spin structure with unequal chirality domain populations.

The squares and triangles in Fig. 3 are the results of the fit to two spiral structures with two different chiralities: a circular spiral spin structure (squares) and an elliptical spin structure (triangles). In the calculation, contributions from two chirality domains are considered at all magnetic Bragg points. For the fitting, the initial polarization was taken to be $P_0=0.92(1)$ in accord with the beam polarization estimated from the nuclear Bragg peak. The first model is the circular spiral model in the ac plane that has no anisotropy in moment size. First, as shown in Fig. 3, the circular spiral model produces P_{yy} and P_{zz} that have signs opposite to those observed at $\mathbf{Q}=(0, 2.1, 1)$, $(0, 1.9, 1)$, and $(0, 2.1, -1)$. For other reflections, the model does not fit the data well either. On the other hand, an elliptical spin model could reproduce the data quite well. The best fit was obtained by an elliptical spiral structure where spins with the same moment lie in the ac plane, with an elongated axis along the c axis. The ratio between the spin component along a (S_a) and along c (S_c) was obtained to be 1.24(1) by fitting the P_{yy} and P_{zz} terms that are related to the difference between S_a and S_c . The different S_a and S_c give rise to an imbalance in polarization, which is not expected in the circular spiral structure. One should note that the chirality terms, P_{yx} and P_{zx} , are also reproduced. The volume ratio between two chirality domains are estimated to be ~ 1.2 , which slightly depends on magnetic domains. We also checked a possibility of the circular spiral structure being tilted along the c axis. In this model, the spin structure projected onto the ac plane is the same as the elliptical spiral structure. However, the calculation based on the model shows that the absolute values of P_{yy} and P_{zz} at $\mathbf{Q}=(3, 1.1, 0)$ and $(3, -0.9, 0)$ cannot be explained since the spin component along the IC vector, which depolarizes P_{yy} and P_{zz} , becomes finite. Therefore, we conclude that the ground state of CdCr_2O_4 has the elliptical spiral structure with the ac planar anisotropy with an elongated axis along the c axis. Since the present polarimetry results are not ascribed to the local spin structure but to the averaged structure, we could not distinguish between the two proposed spin structures with different stacking along the c axis, as shown in Fig. 1.

C. Magnetic field effect

In order to understand the magnetic properties in more detail, we performed neutron-diffraction measurements under an external magnetic field up to 14 T. It is reported that CdCr_2O_4 shows a field-induced transition into a half-magnetization plateau above ~ 28 T.¹⁰ Our experiments were, however, performed well below the critical field, and thus we expect no field-induced phase transition in our measurements. Figure 4 shows the IC magnetic Bragg peak profiles at 5.5 K as a function of H .

The central peak of the triplet at the nominally commensurate position $(0, 2, 1)$ indeed comes from two out-of-plane incommensurate $(\pm\delta, 2, 1)$ reflections. Recall that the polarimetry found that the spins lie on a plane perpendicular to the direction of the incommensurability δ . Therefore, in the

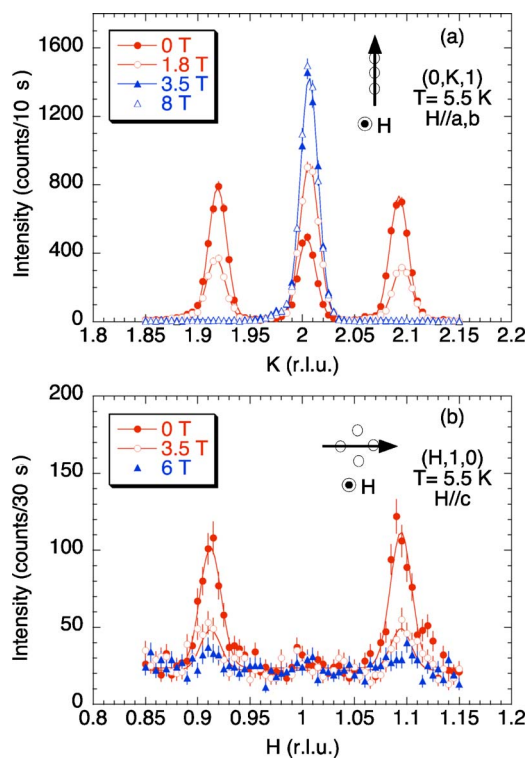


FIG. 4. (Color online) Incommensurate magnetic Bragg peaks around $(0, 2, 1)$ (a) and $(1, 1, 0)$ (b) at 5.5 K. In (a) the positions of the side peaks correspond to $(0, 2 \pm \delta, 1)$. On the other hand, the central peak corresponds to a sum of two peaks at $(\pm\delta, 2, 1)$. The magnetic field is applied along a (or b) in (a) and along c in (b). Scan trajectories are shown in the figure. Magnetic field was applied perpendicular to the scattering plane.

magnetic domains that produce the central peak, the spins lie on the scattering plane that is perpendicular to the external magnetic field. On the other hand, in the domains that produce the two side IC peaks of the triplet [see Fig. 4(a)] and the two IC peaks shown in Fig. 4(b), the spins lie on the plane perpendicular to the scattering plane. Upon increasing the external field, the central peak becomes stronger while other peaks weaken. One may ask if the intensity increase of the central peak is due to a field-induced incommensurate-to-commensurate transition which will shift the peaks closer to the commensurate position and thereby increase the intensity. We have investigated this possibility by performing the similar measurements with a two-dimensional PSD that provides the vertical \mathbf{Q} dependence. The results shown in Fig. 5 clearly show that the magnetic field along the a axis up to 4 T does not change the incommensurability and that there is no incommensurate-to-commensurate transition. These field effects can be qualitatively understood by the rearrangement of the magnetic domain populations depending on the relative angle between the spins and the field: the domains responsible for the central peak is preferable under the field because the spins in those domains are perpendicular to the field.

The critical field for the domain population rearrangement depends on the spin directions as well as on the lattice elongation direction relative to H . For instance, as shown in Fig.

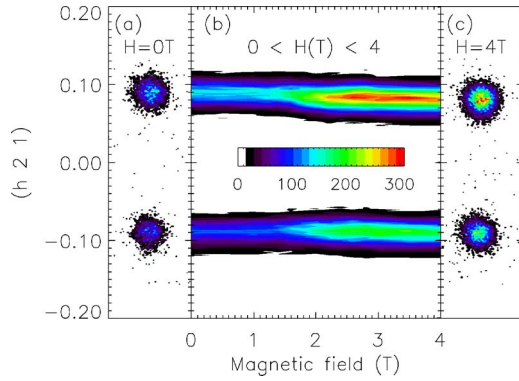


FIG. 5. (Color online) 2D images of the two vertical incommensurate magnetic Bragg peaks around $(0, 2, 1)$ at $H=0$ (a) and 4 T (c) at $T=4.0$ K. (b) Field dependence of the horizontally integrated intensity from the 2D measurement.

6(a), when both the spins and the lattice elongation axis are perpendicular to H , it requires only 2.5 T to rearrange the domain populations. On the other hand, when the lattice elongation axis is parallel to H , as shown in Figs. 4(b) and 6(c), it requires a higher field, ~ 6 T, to make the IC peaks disappear. This higher field is due to the fact that the field-induced spin reorientation and the preferred spin plane determined by the tetragonal distortion are not compatible.

Figure 7 shows the magnetization curves measured at 1.7 K with the crystal pressed along one of the principal axes. Since the c axis is elongated below T_N , it is expected that the c axis points perpendicular to the direction along which the pressure is applied (F). In the case of $H\parallel F$, H is perpendicular to the c axis. On the other hand, in the case of $H\perp F$, H is parallel to the c and a (or b) axes from two magnetic domains. The magnetization curve is almost linear when $H\parallel F$. When $H\perp F$, hysteresis is observed between ~ 0 and ~ 5 T and the magnetization curve becomes almost linear in the ramping down process.

IV. DISCUSSION

As described in Sec. III C, the magnetic-field dependence with H perpendicular to the a axis can be explained by an orientation of the magnetic domains, in which the magnetic domains with spins perpendicular to H are favored. This population change in the magnetic domains is more complex than the simple spin-flop transition. For instance, when $H\parallel a$, the magnetic $(0, \delta, 1)$ Bragg peaks of the triplets completely disappear, while the central peak increases in intensity by a factor ~ 3 . This indicates that the spins not only flip into the bc plane but also reorient to change the direction of the IC wave vector from $(0, \delta, 1)$ to $(\delta, 0, 1)$. The critical magnetic field for the reorientation of the magnetic domain, $H_c \sim 2$ T (~ 0.4 meV), corresponds to an energy barrier between the two degenerate spin spiral states. This energy scale is reasonable because the anisotropy gap of spin wave excitations at the zone center, which was observed in inelastic neutron scattering study, is ~ 0.5 meV.¹²

On the other hand, when H is parallel to the lattice elongation axis (c axis), all the magnetic Bragg peaks in the

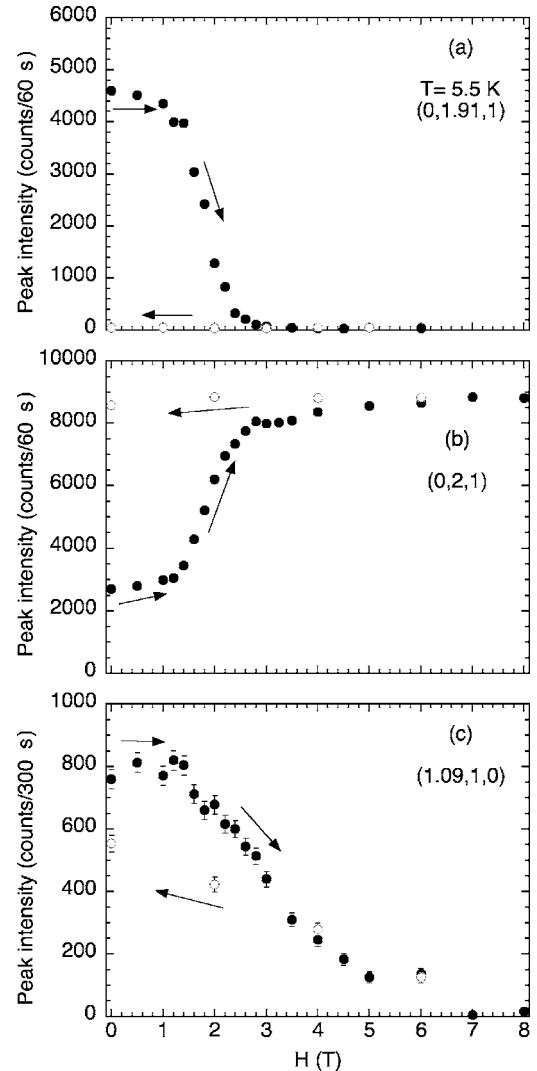


FIG. 6. Magnetic-field dependence of the peak intensity at $(0, 1.91, 1)$, $(0, 2, 0)$, and $(1.09, 1, 0)$ magnetic Bragg reflections at 5.5 K. Filled and open circles represent the data measured when the field increases and decreases, respectively.

quadruplets corresponding to the $(0, \delta, 1)$ or $(\delta, 0, 1)$ domains completely disappeared for $H > \sim 5$ T. The fact that the central peak of the triplet increased in intensity by more than a factor of 2 suggests that the crystal domain responsible for the quadruplets merged into those responsible for the triplets. The fact that the characteristic magnetic field of 5 T (~ 0.9 meV) used to eliminate the quadruplet magnetic peaks is larger than that used to eliminate the triplet peaks supports the scenario of crystallographical domain change when $H\parallel c$. Whether or not this is indeed the case remains to be seen by further studies, such as synchrotron x-ray measurement.

As shown in Sec. III C, when $H\perp F$, the magnetization is smaller in the ramping up process with hysteresis. The range of the hysteresis between ~ 0 and ~ 5 T almost corresponds to the range where the hysteresis is observed in the neutron measurements. These behaviors can be explained if one assumes that the structure becomes slightly orthorhombic under pressure ($c > a > b$ with $F\parallel b$) and that the spins lie on the ac plane perpendicular to F . In the case of $H\perp F$, the mag-

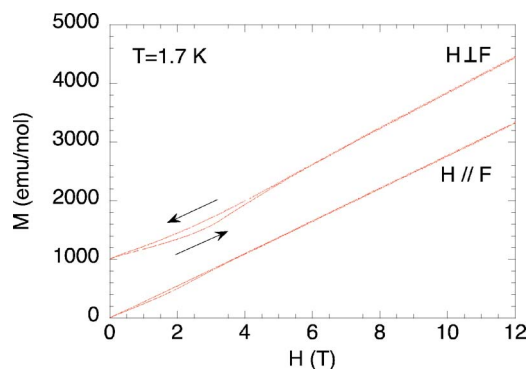


FIG. 7. (Color online) Magnetization curves in CdCr_2O_4 measured at 1.7 K below 12 T. During the measurements, the crystal was pressed along one of the principal axes so that the c axis points perpendicular to the direction. Magnetic field was applied parallel and perpendicular to the direction along which the pressure is applied (F). The data with $H \perp F$ have been displaced vertically by 1000 emu/mol for clarity.

netic field is along the easy plane. Therefore, the hysteresis probably originates from a spin-flop transition, which is accompanied by the change of the crystallographical domain when $H \parallel c$, as described above. In the case of $H \parallel F$, linear magnetization with only small hysteresis is observed, which is expected since all the spins are perpendicular to the magnetic field. All these results are quite consistent with the magnetic structure determined by the present neutron-diffraction study.

What causes the particular spin structure in CdCr_2O_4 with the elliptical spiral in the ac plane, elongated along the c axis and the incommensurability along the b axis? It has been theoretically shown that antisymmetric Dzyaloshinskii-Moriya (DM) interactions would favor a coplanar spiral structure.^{19–21} For instance, Chern *et al.* demonstrated how

the magnetoelastic coupling and further neighbor interactions can favor some particular spiral structures.²⁰ The ellipticity of the spin structure may originate from a slightly uniaxial magnetic anisotropy along the c axis. A full understanding of how this particular spin structure was realized in the tetragonal phase of CdCr_2O_4 requires a detailed account of local lattice distortions in the tetragonal phase. Synchrotron x-ray scattering studies are necessary to determine the tetragonal structure, which is in progress.

In summary, using the newly developed spherical neutron polarimetry, we have studied in detail the magnetic spiral ground state of the frustrated spinel CdCr_2O_4 . We presented two possible elliptical spiral spin structures that can explain our data equally well. The external magnetic-field effect on magnetic Bragg peak intensities can be qualitatively explained by the reorientation of their magnetic domains. The spiral spin structure is most likely induced by antisymmetric DM interaction. A complete understanding of the spin-lattice coupling requires detailed structural studies of the low-temperature tetragonal phase.

ACKNOWLEDGMENTS

We would like to thank Y. Ueda and C. L. Henley for stimulating discussions and Y. Shimojo for technical assistance. The experiment at SPINS was supported by the National Science Foundation under Agreement No. DMR-0454672. This work was partially supported by a Grant-in-Aid for Scientific Research on Priority Areas “High Field Spin Science in 100T” (No. 451) from the Japanese Ministry of Education, Culture, Sports, Science and Technology (MEXT) and a Grant-in-Aid for Scientific Research from the Japan Society for the Promotion of Science. S.-H.L. is partially supported by U.S. DOC through No. NIST-70NANB5H1152.

¹A. Olés, *Phys. Status Solidi A* **3**, 569 (1970).

²H. Shaked, J. M. Hastings, and L. M. Corliss, *Phys. Rev. B* **1**, 3116 (1970).

³S.-H. Lee, C. Broholm, T. H. Kim, W. Ratcliff II, and S.-W. Cheong, *Phys. Rev. Lett.* **84**, 3718 (2000).

⁴S.-H. Lee, C. Broholm, W. Ratcliff, G. Gasparovic, Q. Huang, T. H. Kim, and S.-W. Cheong, *Nature (London)* **418**, 247204 (2002).

⁵M. T. Rovers, P. P. Kyriakou, H. A. Dabkowska, G. M. Luke, M. I. Larkin, and A. T. Savici, *Phys. Rev. B* **66**, 174434 (2002).

⁶R. Moessner and J. T. Chalker, *Phys. Rev. Lett.* **80**, 2929 (1998); *Phys. Rev. B* **58**, 12049 (1998).

⁷B. Canals and C. Lacroix, *Phys. Rev. Lett.* **80**, 2933 (1998); *Phys. Rev. B* **61**, 1149 (2000).

⁸A. P. Ramirez, in *Handbook of Magnetic Materials*, edited by K. H. J. Buschow (Elsevier, Amsterdam, 2001), Vol. 13, pp. 423–520.

⁹N. Menyuk, K. Dwight, R. J. Arnott, and A. Wold, *J. Appl. Phys.* **37**, 1387 (1966).

¹⁰H. Ueda, H. A. Katori, H. Mitamura, T. Goto, and H. Takagi, *Phys. Rev. Lett.* **94**, 047202 (2005).

¹¹S.-H. Lee (unpublished).

¹²J.-H. Chung, M. Matsuda, S.-H. Lee, K. Kakurai, H. Ueda, T. J. Sato, H. Takagi, K.-P. Hong, and S. Park, *Phys. Rev. Lett.* **95**, 247204 (2005).

¹³M. Takeda, M. Nakamura, K. Kakurai, E. Lelièvre-Berna, F. Tasset, and L.-P. Regnault, *Physica B* **356**, 136 (2005).

¹⁴F. Tasset, *Physica B* **156-157**, 627 (1989).

¹⁵F. Tasset, P. J. Brown, E. Lelièvre-Berna, T. Roberts, S. Pujol, J. Allibon, and E. Bourgeat-Lami, *Physica B* **267-268**, 69 (1999).

¹⁶L.-P. Regnault, B. Geffray, P. Fouilloux, B. Longuet, F. Mantegazza, F. Tasset, E. Lelièvre-Berna, E. Bourgeat-Lami, M. Thomas, and Y. Gilbert, *Physica B* **335**, 255 (2003).

¹⁷P. J. Brown, J. Crangle, K.-U. Neumann, J. G. Smith, and K. R. A. Ziebeck, *J. Phys.: Condens. Matter* **9**, 4729 (1997).

¹⁸P. J. Brown, J. B. Forsyth, and F. Tasset, *J. Phys.: Condens. Matter* **10**, 663 (1998).

¹⁹M. Elhajal, B. Canals, R. Sunyer, and C. Lacroix, *Phys. Rev. B* **71**, 094420 (2005).

²⁰G.-W. Chern, C. J. Fennie, and O. Tchernyshyov, *Phys. Rev. B* **74**, 060405(R) (2006).

²¹C. L. Henley (private communication).